CellPress

Neuron
Article

# Identifying Functional Connections of the Inner Photoreceptors in *Drosophila* using Tango-Trace

Smitha Jagadish,[1] Gilad Barnea,[2] Thomas R. Clandinin,[3,*] and Richard Axel[1,*]
[1]Department of Neuroscience and the Howard Hughes Medical Institute, College of Physicians and Surgeons, Columbia University, New York, NY 10032, USA
[2]Department of Neuroscience, Brown University, Providence, RI 02912 USA
[3]Department of Neurobiology, Stanford University, Stanford, CA 94305, USA
*Correspondence: trc@stanford.edu (T.R.C.), ra27@columbia.edu (R.A.)
http://dx.doi.org/10.1016/j.neuron.2014.06.025

## SUMMARY

**In *Drosophila*, the four inner photoreceptor neurons exhibit overlapping but distinct spectral sensitivities and mediate behaviors that reflect spectral preference. We developed a genetic strategy, Tango-Trace, that has permitted the identification of the connections of the four chromatic photoreceptors. Each of the four stochastically distributed chromatic photoreceptor subtypes make distinct connections in the medulla with four different TmY cells. Moreover, each class of TmY cells forms a retinotopic map in both the medulla and the lobula complex, generating four overlapping topographic maps that could carry different color information. Thus, the four inner photoreceptors transmit spectral information through distinct channels that may converge in both the medulla and lobula complex. These projections could provide an anatomic basis for color vision and may relay information about color to motion sensitive areas. Moreover, the Tango-Trace strategy we used may be applied more generally to identify neural circuits in the fly brain.**

## INTRODUCTION

Visual stimuli are detected by photoreceptors in the retina and transmitted to the brain to generate an internal representation of the visual world. The brain must then translate this representation of stimulus features into visually guided behaviors (Johansso, 1973). In *Drosophila*, the retina resembles a crystalline lattice comprised of 750 precisely ordered units, the ommatidia. Each ommatidium contains eight photoreceptor neurons (R1–R8). The outer photoreceptor neurons, R1–R6, express the Rh1 opsin and are thought to receive achromatic visual stimuli that ultimately inform the fly about the form, position, and movement of objects in the visual world. There are two types of ommatidia that differ in the opsins expressed by the inner photoreceptor, R7 and R8 (Franceschini et al., 1981; Wernet and Desplan, 2004). In Pale (p) ommatidia, R7 expresses the near UV-sensitive opsin Rh3 and the R8 cell expresses the blue-sensitive opsin Rh5. In Yellow (y) ommatidia, R7 cells contain the far UV-sensitive opsin Rh4, whereas the R8 cell expresses the green-sensitive opsin Rh6.

The existence of the four types of inner photoreceptor neurons, each with overlapping but distinct spectral sensitivities, has implicated these neurons in the recognition of chromatic visual information (Buchner et al., 1984; Heisenberg, 1977). *Drosophila* exhibit phototactic behaviors, strongly preferring UV to green light, a preference that is not observed in flies in which neurotransmitter release is blocked in R7 cells (Gao et al., 2008; Yamaguchi et al., 2010). These observations suggest that the chromatic inner photoreceptors elicit behaviors that reflect spectral preference, but the response to light of distinct wavelengths does not constitute color vision.

Color vision requires the ability to distinguish light of distinct spectral composition independent of intensity. The principle of univariance argues that a single photoreceptor cannot distinguish different wavelengths from different intensities of light (Rushton, 1972). Color vision therefore requires a neural system capable of comparing the inputs from photoreceptor neurons in the retina that exhibit different spectral sensitivities (Hurvich and Jameson, 1957; Livingstone and Hubel, 1984). In mammals, this comparison is apparent early in the visual pathway, with a subset of retinal ganglion cells exhibiting color opponency, a feature that reflects opposing neural responses to input from different types of photoreceptor cells (Livingstone and Hubel, 1984; Masland, 2001). In flies, connections between photoreceptors do not facilitate a comparison of inputs (Shaw, 1984). Color vision would therefore require a comparison of different photoreceptor inputs in downstream visual processing centers. However, the connections of the four inner photoreceptors are largely unidentified and it is unknown whether p and y ommatidia project to identical or distinct downstream circuits.

The achromatic R1–R6 neurons project axons to cartridges within the lamina, an optic lobe structure immediately below the retina (Meinertzhagen and O'Neil, 1991). The R7 and R8 axons course through the lamina and synapse on second-order neurons within a column in the medulla. The R7 and R8 cells from a single ommatidium project axons to the same column and the topographic organization of the columns maintains retinotopic order (Clandinin and Zipursky, 2002; Sanes and Zipursky, 2010). Anatomic studies continue to reveal a vast complexity of richly arborizing intrinsic neurons and projection neurons in

the medulla that have seriously hindered the identification of synaptic partners of R7 and R8 neurons. EM studies suggest connections between R7, a medullary projection neuron Tm5 and a medullary intrinsic neuron Dm8 (Gao et al., 2008; Takemura et al., 2013). Moreover, genetic studies have shown that Dm8 is necessary for UV spectral preference (Gao et al., 2008). Tm neurons in the medulla project their axons to only one of the two neuropils of the lobula complex. TmY cells in the medulla project a branched axon to both the lobula and the lobula plate (Fischbach and Dittrich, 1989; Raghu and Borst, 2011; Varija Raghu et al., 2011). The lobula plate contains neurons that respond strongly to motion (Farrow et al., 2003; Haag and Borst, 2003, 2008; Joesch et al., 2008) and loom sensitive neurons have been identified in the lobula plate (de Vries and Clandinin, 2012), but the function of the remaining neural structures within the lobula complex remains obscure.

In other insects such as bees that exhibit clear behavioral evidence for color vision, color opponent neurons have been identified with electrophysiologic recordings in the inner layers of both the medulla and lobula as well as by imaging studies in the anterior optic tubercle (Kien and Menzel, 1977; Mota et al., 2013; Paulk et al., 2008, 2009; Paulk and Gronenberg, 2008; Riehle, 1981; Yang et al., 2004). Color opponent neurons provide an anatomic substrate for a comparison of the different photoreceptors. Efforts to identify the chromatic neural circuits that could underlie color vision in *Drosophila* have failed to identify color opponent neurons in the optic lobe. Moreover, behavioral studies have not provided convincing evidence for color vision in the fly.

We developed a genetic strategy, Tango-Trace, which permits us to trace functional synaptic connections of the R7 and R8 photoreceptor neurons in the optic lobe of *Drosophila*. Our studies reveal that each of the four stochastically distributed chromatic photoreceptor subtypes makes a different functional synaptic connection with four different TmY cells in the medulla. The four distinct TmY cells all project to the innermost layer of the lobula and extend axons more diffusely to multiple layers within the lobula plate. The observation that the four inner photoreceptors transmit spectral information through distinct channels that can connect to one another in both the medulla and the lobula complex may provide the anatomic substrate for color vision. Moreover, the Tango-Trace strategy used to trace connections in the dense medullary neuropil may be applied more generally to identify neural circuits in the fly brain.

## RESULTS

### Histamine Tango Assay Detects Histamine Release in the Visual System

*Drosophila* photoreceptor neurons use histamine (HA) as the primary neurotransmitter at synapses in the lamina and medulla. We developed a genetic strategy to detect the synaptic release of HA, an approach designed to identify the postsynaptic targets of specific photoreceptor neurons. This experimental strategy, Tango-Trace, is based on the Tango assay (Barnea et al., 2008) in which a transient G protein-coupled (GPCR) receptor-ligand interaction results in a stable transcriptional readout. In *Drosophila*, the known HA receptors, *outer rhabdomeres transientless* (*ort*; *HisC12*) and *HisC11* are chloride channels (Gengs et al., 2002; Gisselmann et al., 2002; Witte et al., 2002). The human HA receptor 2 (HRH2) is a GPCR that exhibits a pharmacological profile similar to the *Drosophila* HA receptor, *ort* (Buchner et al., 1993; Roeder, 2003; Sarthy, 1991; Stark, 2003), suggesting that heterologous expression of HRH2 in Tango-Trace could be used to detect endogenous HA release in flies.

We therefore generated a fusion protein (HRH2-TCS-Gal4), consisting of HRH2 joined at its C terminus to the transcriptional activator, Gal4. Interposed between these sequences, we introduced the cleavage site (TCS) for a specific protease, N1a, from the Tobacco Etch Virus (TEV). Ligand activation of GPCRs results in recruitment of the cytosolic protein, arrestin, to the activated receptor. We therefore generated a second fusion protein consisting of the TEV protease linked to human β-arrestin 2 (Arr-TEV). Ligand-dependent recruitment of Arr-TEV to the receptor fusion, HRH2-TCS-Gal4, leads to cleavage at the TCS releasing Gal4 from the membrane. Translocation of Gal4 to the nucleus then induces expression of transgenes controlled by the Gal4-dependent, upstream activating sequence (UAS; Figure 1A).

We introduced the histamine Tango system into flies by generating animals expressing HRH2-TCS-Gal4 and Arr-TEV under the control of the tubulin promoter (Tubp). These flies also contain the reporter construct *UAS mCD8-GFP*. In flies containing these three transgenes (HA-Tango flies), neurons exposed to HA should express CD8-GFP, allowing the visualization of their cell bodies and axonal and dendritic projections. HA-Tango flies were reared in the dark and then exposed to 10 s light flashes for 3 min (Figure 1B; n = 12; Figures S1 and S2 available online). After 16 hr, the optic lobes were examined for the expression of CD8-GFP by whole mount immunohistochemistry with antibodies directed against GFP. Control flies were either reared in the dark (Figure 1D; n = 8) or maintained in ambient light without exposure to light flashes (Figure 1C; n = 12). In dark-reared flies exposed to light flashes, we observed GFP expression in cell bodies surrounding the lamina and medulla, as well as in processes extending into the lobula and lobula plate. In the lamina, we observed strong GFP expression in the histamine-receptive LMC neurons that receive synaptic inputs from R1-6. In the medulla, labeled cell bodies were observed in the distal medulla and their projections extended to several layers of the medulla and the lobula complex. Intense GFP staining was also observed in glia surrounding these neuropils. Dark- reared flies and flies reared in ambient light exhibited significantly lower levels of GFP staining (Figure 1G).

Expression of CD8-GFP depended on the coordinate expression both of HRH2-TCS-Gal4 and Arr-TEV fusion proteins. GFP expression was not detected in control flies that express HRH2-TCS-Gal4 in the absence of Arr-TEV (Figure 1E; n = 9). The dependence on HA was examined by introducing HRH2-Gal4 and Arr-TEV into flies homozygous for a hypomorphic mutation in histidine decarboxylase (hdc) that results in a dramatic reduction in HA release (Melzig et al., 1996). In this genetic background, HA-Tango-induced GFP expression was significantly reduced in neurons of the optic lobe (Figure 1F; n = 8). These experiments demonstrate that light-induced HA release results in

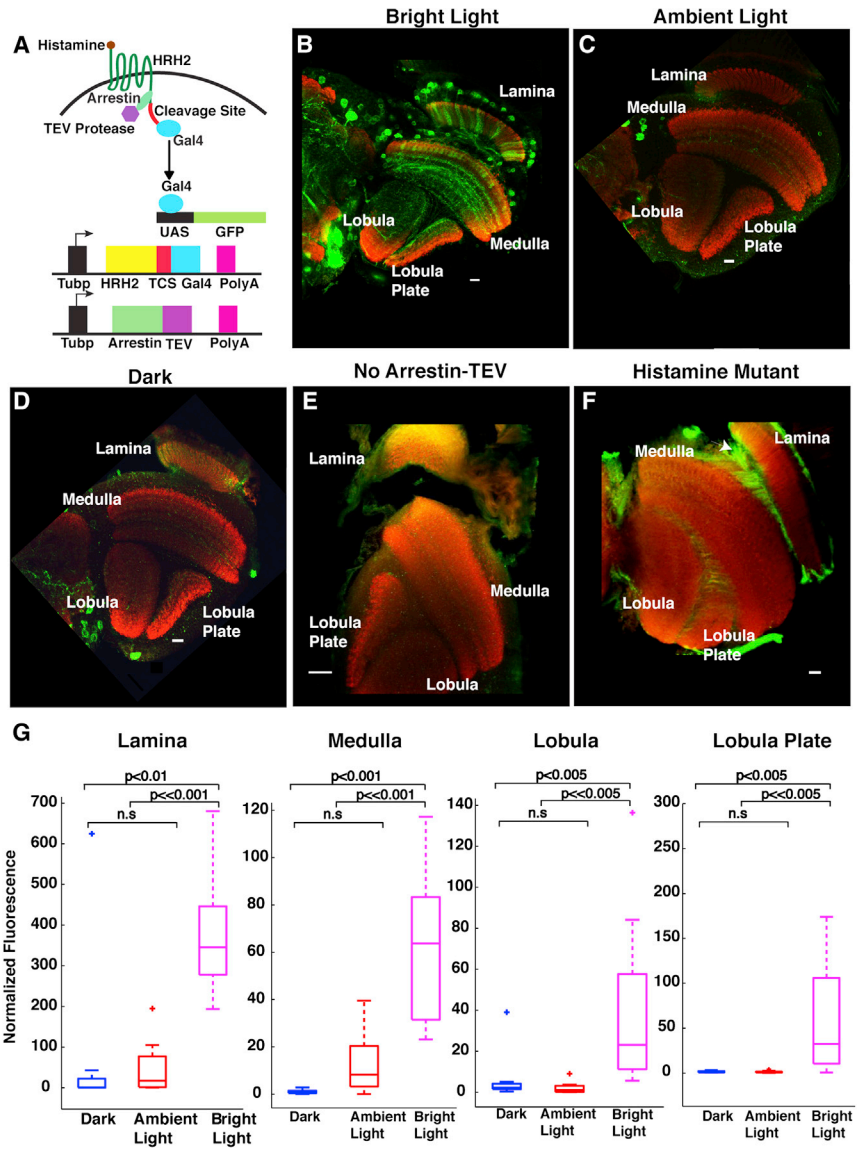


**Figure 1. Light-Dependent Labeling of Neurons in the Fly Visual System by Histamine-Tango**

(A) Schematic illustration of the Histamine (HA)-Tango assay. A human HA receptor (HRH2) was fused to Gal4, interposed by the cleavage site (TCS) for a specific protease from Tobacco Etch Virus (TEV). A second transgene encoding human β-arrestin2 was fused to TEV protease at its C terminus. The HA-Tango constructs were expressed ubiquitously under the control of the α-tubulin promoter (Tubp).

(B–D) HA-Tango detects light dependent release of histamine in the visual system. HA-Tango transgenes were expressed in flies expressing Tubp Gal80$^{ts}$. Flies were reared in the dark, shifted to 30°C for 18 hr, and exposed to 10 s light flashes for 3 min (B; n = 12). Control flies were reared in ambient light (C; n = 12) or in the dark (D; n = 8), without exposure to light flashes, and shifted to 30°C for 18 hr. Flies were then placed at 25°C overnight, fixed, and stained.

(E and F) GFP expression was reduced in HA-Tango flies that do not contain the arrestin-TEV transgene (E; n = 9), exposed to light flashes and stained as described in (B). Flies that express a hypomorphic *Histamine decarboxylase* (*Hdc*) and exhibit diminished histamine levels (F; n = 8) were exposed to light and stained as above. Scale bar represents 20 μm in (E) and 10 μm in (B–D and F). Arrow in (F) indicates HA-Tango labeling in glia. Whole mount brains were immunostained with mouse nc82 in red and with rabbit anti-GFP in green.

(G) Box plots of the quantification of GFP fluorescence in (B–D) in the lamina, medulla, lobula, and lobula plate. The top and bottom boxes of each plot are the 25$^{th}$ and 75$^{th}$ percentiles of the samples. The middle bar denotes the median, the upper and lower whiskers extend up to 1.5 times the interquartile range. p values represent Wilcoxon rank-sum test. Error bars denote ± 2 SD of the mean. See also Figures S1 and S2.

GFP expression in histamine receptive neurons in the optic lobe in HA-Tango flies.

## Genetic Control of Histamine Release in Specific Neurons

The identification and characterization of neurons postsynaptic to individual photoreceptors requires genetic manipulation to elicit HA release from small subpopulations of identified photoreceptor cells. Pale and yellow R7 and R8 photoreceptor neurons each express a distinct rhodopsin gene. The promoters of each of the four different rhodopsins were used to drive expression of the temperature-sensitive cation channel, dTrpA1, in p/y R7 and R8 cells, permitting heat induction of HA release by the individual photoreceptor neurons. Heat-induced HA release from yR7 cells driven by *Rh4-Gal4* in HA-Tango flies results in strong GFP expression in both cell bodies and processes in the medulla as well as in processes terminating in the lobula and lobula plate (Figure 2A; n = 5). Arborization (presumably of dendrites) in the medulla was most extensive in layers 7–10. In the lobula plate, arborization was distributed throughout many layers, whereas in the lobula, the projections appear to be restricted to the innermost layer. A similar pattern of GFP expression in both cell bodies and processes is observed in flies in which dTrpA1 was driven by each of the four rhodopsin promoters (Figure 2B; n = 4, and data not shown). Expression of GFP was dramatically reduced in the cells of the optic lobe in these strains without heat exposure (Figure 2C; n = 7). Moreover, control flies that contain the HA-Tango transgenes, but did not harbor the dTrpA1 transgene, exhibit little or no GFP labeling upon exposure to heat (Figure 2D; n = 10). Thus, genetic control of HA release in individual photoreceptor subtypes should permit the characterization of their postsynaptic partners in the medulla and the projections of these postsynaptic neurons in the lobula complex.

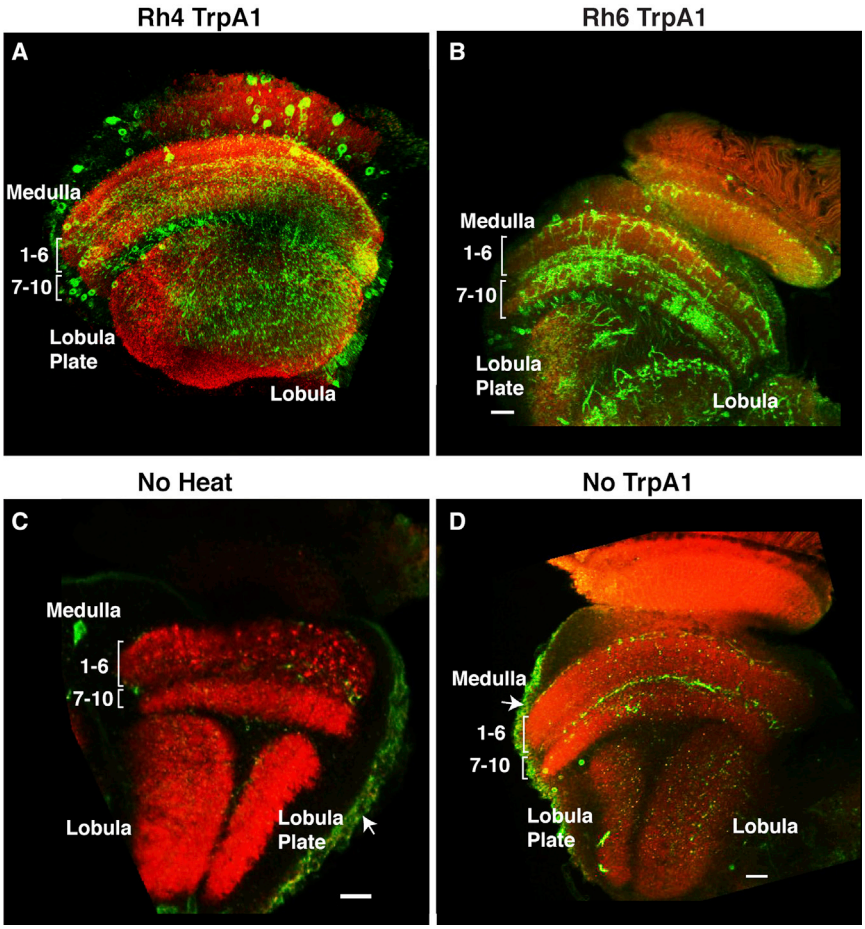


**Figure 2. Genetic Control of Histamine Tango Labeling in the Fly Visual System**

(A) HA-Tango-Trace flies expressing dTrpA1 in yR7 cells driven by *Rh4 Gal4* were warmed to 37°C, resulting in GFP expression in both cell bodies and processes in the medulla as well as in processes terminating in the lobula and lobula plate (n = 5).

(B) HA-Tango-Trace flies expressing dTrpA1 in yR8 cells driven by *Rh6 Gal4* when warmed to 37°C also exhibit labeling in the medulla and lobula complex (n = 4).

(C) HA-Tango-Trace flies expressing dTrpA1 driven by *Rh4 Gal4*, but not exposed to heat exhibit little or no GFP labeling (n = 7).

(D) HA-Tango-Trace flies that do not harbor the dTrpA1 transgene exhibit only weak GFP expression after exposure to 37°C (n = 10).

Brains were stained (see Experimental Procedures) with mouse nc82 in red and rabbit anti-GFP in green. Scale bar represents 10 μm in (A), (B), and (D) and 20 μm in (C). Arrows indicate HA-Tango labeling in glia surrounding the neuropils.

## Visualizing the Projections of the Postsynaptic Partners of Individual R7 and R8 Neurons

We performed mosaic analysis with a repressible cell marker (MARCM; Lee and Luo, 1999) to visualize CD8-GFP expression in sparse populations of postsynaptic neurons in HA-Tango flies. The sparse labeling of neurons responsive to the activation of each of the photoreceptors should allow the identification of individual postsynaptic partners of the individual inner photoreceptors. We generated flies that carry the HA-Tango-Trace transgenes, along with the transgenes facilitating MARCM. In MARCM, the loss of the transcriptional repressor Gal80 in a small subpopulation of neurons was achieved by FLP/FRT-mediated interchromosomal recombination, induced by heat shock during development. HA release was elicited in photoreceptors expressing dTrpA1 by gradually warming adult flies to 37°C (see Experimental Procedures). This approach required MARCM clones of R cells as the starter cells for HA-Tango-Trace labeling. In these flies, mCD8-GFP was expressed in a sparse population of neurons that were labeled by HA-Tango-Trace, allowing the visualization of the dendritic and axonal arbors of individual labeled postsynaptic neurons. This strategy also labels the presynaptic photoreceptors in which *Rh-Gal4* drives the *UAS mCD8-GFP* reporter. Examination of over 3,000 fly brains allowed us to see the patterns of projections of 1697 individual postsynaptic targets of the inner photoreceptors from their presumed dendritic arbor in the medulla to their axonal target in the lobula complex.

Analysis of the dendritic projections of the 1,697 individual postsynaptic targets of R7 and R8 in the medulla revealed several interesting features. First, the inner photoreceptors, p/y R7 and R8 each synapse on one of four distinct TmY cells. Each photoreceptor subtype contacts a unique postsynaptic TmY target, Rh3TmY, Rh4TmY, Rh5TmY, and Rh6 TmY (Figures 3A–3D, S3, and S4). The four TmY neurons project to the same layers (7–10) in the proximal medulla, but exhibit distinct arborizations that characterize the four TmY cell types. Each of the four TmY cells project to the lobula and lobula plate in a columnar manner presumably maintaining retinotopy in these structures (Figures 5, 7, S6, and S7). All the TmY cells we have identified project to all four layers of the lobula plate, but their projections are restricted to the innermost layer of the lobula. The projection patterns of the four TmY cells are nonetheless anatomically distinct and conserved across animals examined. These cells have not been described in previous studies using Golgi staining (Fischbach and Dittrich, 1989). The overall morphology of these cells resembles a recently characterized cell type, $TmY^{new1}$, identified using a Gal4 line that labels glutamatergic cells (Raghu and Borst, 2011).

We also observed an amacrine cell, Dm8, which is postsynaptic to all the inner photoreceptor subtypes (Figures 4A–4E and S5). Dm8 was previously identified as a postsynaptic target of R7 necessary for UV phototaxis (Gao et al., 2008). Dm8 is a wide field amacrine cell contacting 14–15 columns in both the anterior-posterior (AP) and dorsal-ventral (DV) axes in layer 6 of the distal medulla and was shown to be involved in UV phototaxis. The p/y R7 and R8 photoreceptors also contact an intrinsic medullary cell, Mia (Figures 4F–4J). This cell type resembles the $Mi^{new2}$ cell that was identified using the *dvGluT-Gal4* line (Raghu

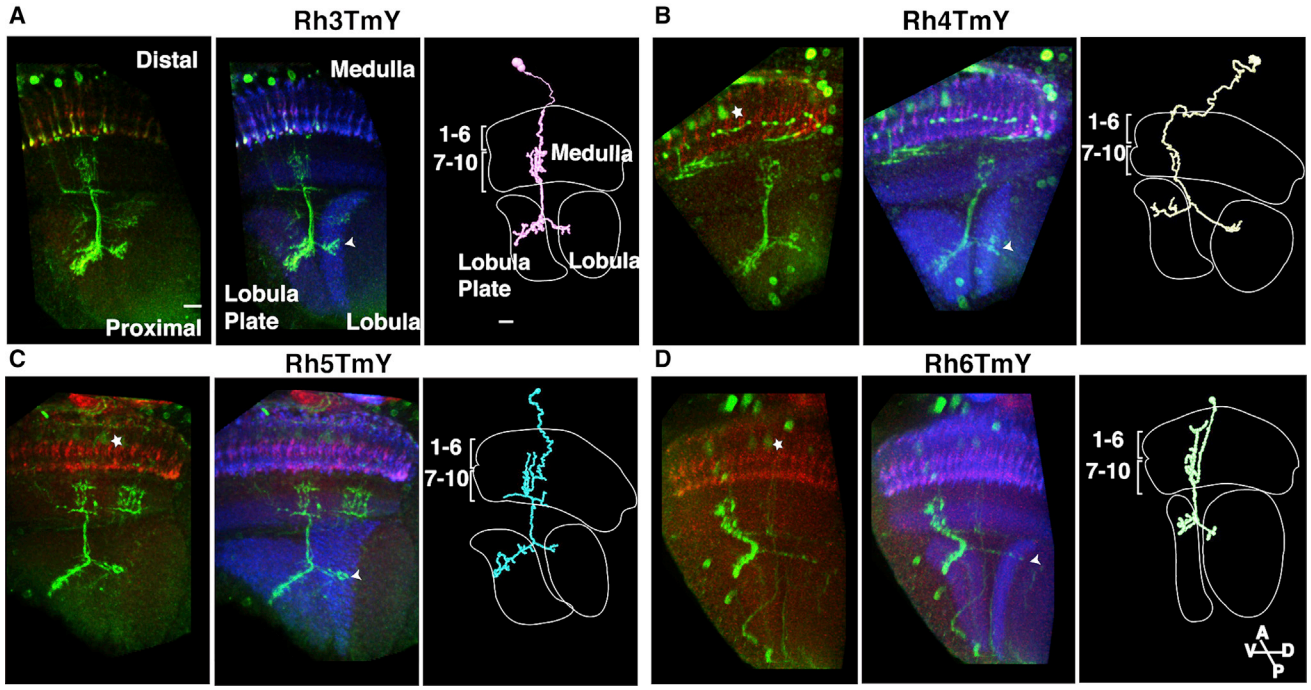


**Figure 3. Visualizing the Projections of Postsynaptic Partners of Individual R7 and R8 Photoreceptors**

(A–D) HA-Tango-Trace was combined with MARCM to depict CD8-GFP expression in sparse populations of postsynaptic neurons. (A) Rh3TmY, (B) Rh4TmY, (C) Rh5TmY, and (D) Rh6TmY. MARCM clones were generated by heat shock during development (see Experimental Procedures) and HA-Tango-Trace labeling was performed as described in Figure 2. Brains were immunostained with anti-GFP (green), the neuropil marker anti-Csp2a (blue), and photoreceptor marker mAb24B10 (red). Images were rendered in Imaris for demonstration of TmY cell morphology. Semi-automated neurite tracings of TmY cells were done in the skeleton tree module in Amira (see Supplemental Experimental Procedures). Arrowheads indicate the most medial lobula layer where the axons project, which is also labeled by the Csp2a antibody. The LMC L2 was also labeled by HA-Tango-Trace although light changes were kept to a minimum (asterisk). Scale bars represent 10 μm.

See also Figures S3 and S4.

and Borst, 2011), and innervates four to five columns in the DV axis in layers 7-9 of the proximal medulla. In layer 1 of the distal medulla, Mia contacts 14–15 columns in both the AP and DV axes. In each *Rh-Gal4* line, the four unique TmY cells identified by HA-Tango-Trace are observed 10-fold more frequently (346 ± 58, n = 45; Figures 5A and 5B) than Dm8 (33 ± 10, n = 24; Figures 5A and 5B) or Mia (46 ± 23, n = 24; Figures 5A and 5B). Rarely, we labeled the previously described cell types Mil (n = 3) and Tm20 (n = 2), the postsynaptic partners of yR8 (Figure S5; Takemura et al., 2013).

This tracing strategy labels the postsynaptic partners of the p/y R7 and R8 photoreceptors as well as the R7 and R8 cells themselves, because these flies carry an *Rh-Gal4* driver along with *UAS-mCD8-GFP*. It is therefore possible to examine the projections from a TmY cell in the medulla into a labeled column. We observed that each of the four TmY cells sends projections to two to three neighboring columns (Figures 3, S3, and S4). Although each TmY innervates two to three distinct columns, the photoreceptor in only one of these columns was labeled by our Tango-Trace strategy. Therefore, we cannot identify the photoreceptor type in the unlabeled columns.

Analysis of the patterns of columnar innervation suggests that a TmY postsynaptic to a given photoreceptor type also innervates columns that receive input from different photoreceptors. In brains in which 5–20 TmY cells are labeled, the projections of the TmY cells innervate columns in a contiguous manner. We extracted isosurfaces of GFP staining in densely labeled brains with multiple TmYs (Figures 5C1 and 5E). Regions of these extracted isosurfaces were selected for analysis of the columnar distribution of TmY cell projections in the proximal medulla (Figure 5C2). The isosurfaces were then registered on a reference optic lobe with Csp2a staining that distinctly labels columns in the medulla (Figure 5D). The contiguity in columnar distribution was analyzed by counting the number of columns contacted by the TmY cells in a square defined by the centers of eight medulla columns (Figure 5C2). We observe that the projections of TmY cells innervate columns in the proximal medulla in a contiguous manner with no apparent preference for columns of any particular type (Figure 5F). If a given TmY cell received photoreceptor inputs from the same column type, the column coverage would not be contiguous, but rather stochastic. Because a given TmY is activated by only one photoreceptor type, this suggests that a TmY cell receives direct photoreceptor input from only one column and extend lateral processes to neighboring columns that are unlikely to receive histaminergic photoreceptor input.

TmY cells of a given type extend contiguously across the entire medulla. When two TmY cells of the same type are in close proximity in the medulla, the processes may overlap in a single

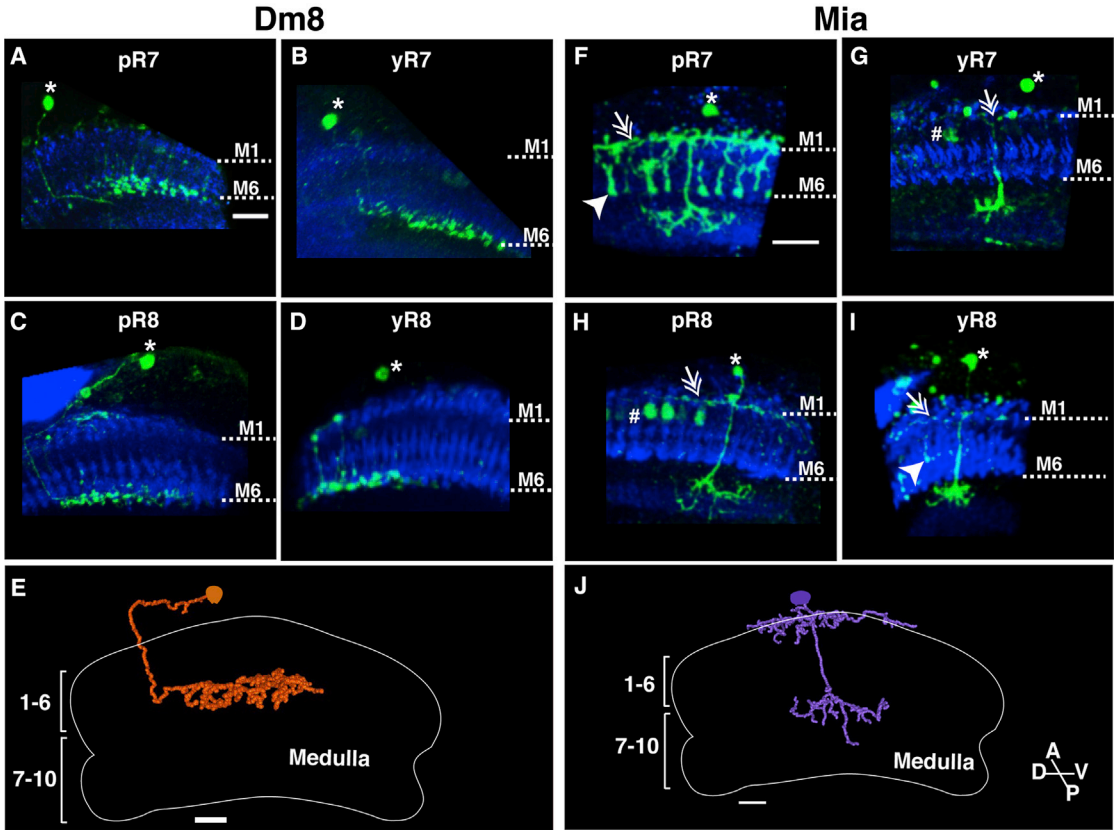


**Figure 4. Visualizing the Projections of Individual Amacrine Postsynaptic Partners of R7 and R8**

(A–E) HA-Tango-Trace combined with MARCM as described in Figure 3 identifies an amacrine cell, Dm8, which is postsynaptic to all the inner photoreceptor subtypes. Dm8 is a wide-field amacrine cell contacting 13–15 columns in layer 6 of the medulla and was identified as a postsynaptic target of pR7 (A), yR7 (B), pR8 (C), and yR8 (D). Semi-automated neurite tracing of a representative Dm8 (E).

(F–J) The inner photoreceptors, pR7 (F), yR7 (G), pR8 (H), and yR8 (I) also contact Mia, a narrow-field amacrine cell contacting 4–5 columns in layer 8 of proximal medulla. Semi-automated neurite tracing of a representative Mia (J). Brains were immunostained with anti-GFP (green), the neuropil marker anti-Csp2a (blue). Semi-automated neurite tracings were performed as described in Figure 3. Asterisks indicate the cell bodies of Dm8 and Mia. Arrowheads indicate photoreceptor termini, double arrows indicate the arborization of Mia in the distal medulla and L2 (hash symbol). Scale bars represent 20 μm.

See also Figure S5.

column. This overlap is maintained in the neighboring columns of the lobula (see below and Figure S7).

We have calculated the ratio of labeled presynaptic and postsynaptic cells observed in HA-Tango-Trace. The ratio of labeled photoreceptor to the cognate TmY cell is 3.3 for Rh3TmY, 2 for Rh4TmY, 2.7 for Rh5TmY, and 4.3 for Rh6TmY. If a given TmY receives input from a single type of photoreceptor from one column, these data imply that the efficiency of Tango-Trace labeling of the postsynaptic partners of the photoreceptors can be high, ranging from 23% to 50%.

It is possible that the MARCM strategy we used to obtain sparse labeling in HA-Tango-Trace resulted in the nonrandom labeling of postsynaptic targets. Nonrandom expression of the genetic elements of the HA-Tango-Trace could affect the relative frequency of identified postsynaptic targets or obscure additional targets. We therefore obtained sparse labeling in HA-Tango-Trace using FLP-mediated excision of a cassette encoding Gal80 under the control of the tubulin promoter (gift from Gary Struhl). Excision of Gal80 was mediated by a mild heat shock during late third instar, a stage when the neurons are postmitotic and specified. Analysis of 200 fly brains and 125 individual labeled postsynaptic targets of the inner photoreceptors again reveals four unique TmYs, Dm8, and Mia as the predominant postsynaptic targets at frequencies similar to that obtained using the MARCM approach. No additional targets were revealed (data not shown). Thus, the restricted set of postsynaptic targets of the inner photoreceptor neurons we observe is unlikely to be a consequence of nonrandom labeling. There are however several additional cell types identified with electron microscopic (EM) reconstruction (Takemura et al., 2013), and it is important to emphasize that additional targets may exist that were not revealed by HA-Tango-Trace.

## Projections of the Individual TmY Cells in the Lobula Complex

The sparse labeling of neurons using HA-Tango-Trace permits a more detailed analysis of the projections of each of the four unique TmY cells in the optic lobe. For example, comparison

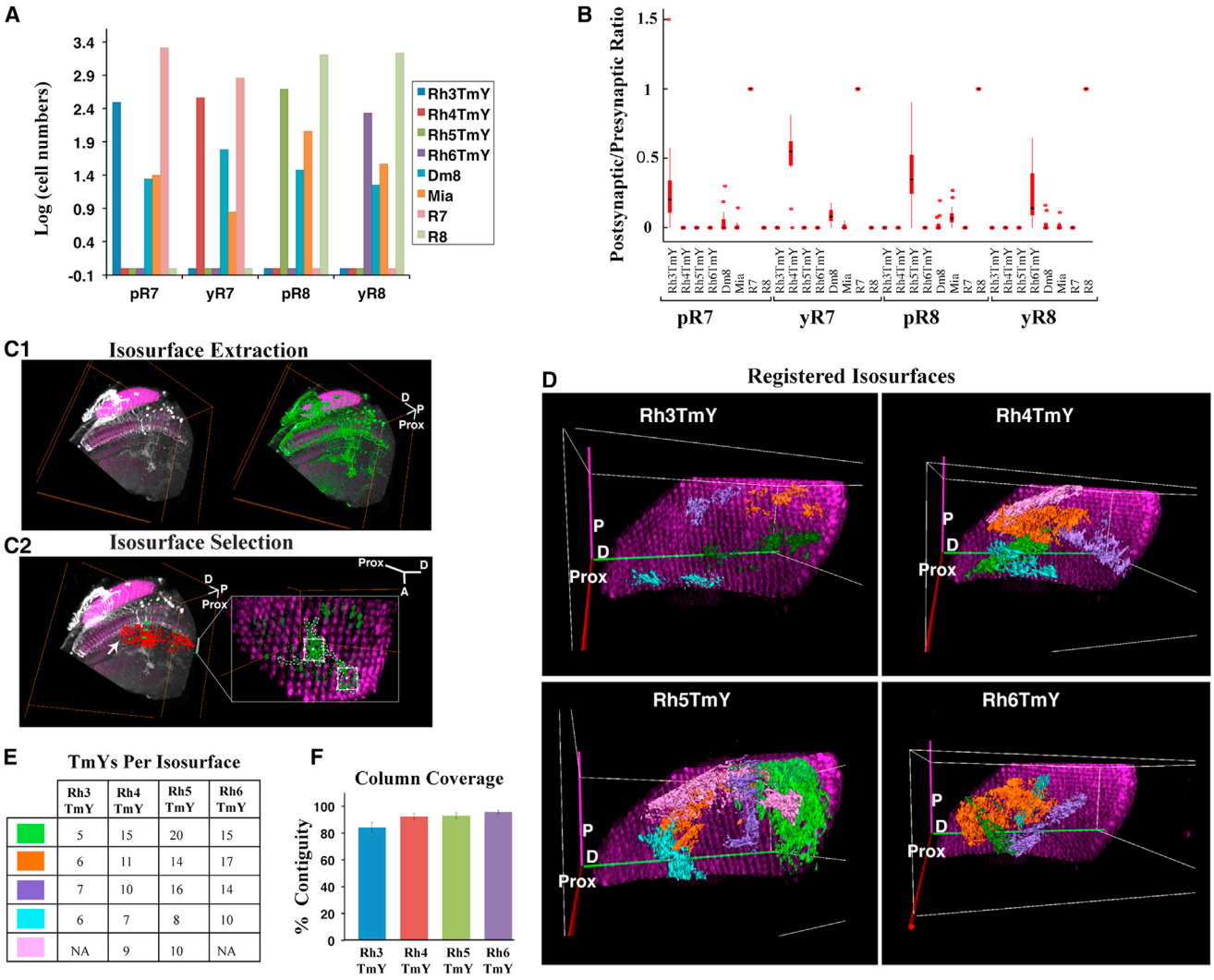


| | Rh3 TmY | Rh4 TmY | Rh5 TmY | Rh6 TmY |
|---|---|---|---|---|
| | 5 | 15 | 20 | 15 |
| | 6 | 11 | 14 | 17 |
| | 7 | 10 | 16 | 14 |
| | 6 | 7 | 8 | 10 |
| | NA | 9 | 10 | NA |

**Figure 5. Quantitative Analysis of HA-Tango-Trace Labeling**

(A) Quantitative analysis of the photoreceptors p/y R7 and R8 and their postsynaptic partners (shown in Figures 3and 4). HA-Tango-Trace labeled neurons are grouped based upon the presynaptic photoreceptor subtype expressing dTrpA1 driven by specific *Rh Gal4* drivers. Analysis was performed on 1697 individual postsynaptic targets of p/y R7 and R8 from a total data set of 7780 neurons expressing CD8-GFP, which included the presynaptic photoreceptors.

(B) The ratio of labeled postsynaptic partners to presynaptic photoreceptors expressing CD8-GFP in the same fly. The distribution of ratios in the data set are grouped according to their presynaptic partner. Analysis was performed on 47 individual flies. A value of 1 for this quotient would indicate that for a given cell type, HA-Tango-Trace labels a cognate postsynaptic cell in a medulla column for every labeled presynaptic photoreceptor in that column. The middle black filled circle denotes the median, the upper and lower whiskers extend to 1.5 times the interquartile range and points exceeding that are marked as outliers (red open circles). Error bars denote ± 2 SD of the mean.

(C) A representative isosurface extraction of densely labeled TmY cells. HA-Tango-Trace labeling was performed as described in Figure 2. Brains were immunostained with anti-GFP (white), and the neuropil marker anti-Csp2a (magenta). Images were rendered in Amira for isosurface extraction of HA-Tango-Trace labeled neurons (A1 and see Supplemental Experimental Procedures). Extracted isosurfaces were registered to a reference optic lobe in Amira (see Supplemental Experimental Procedures). To distinguish the isosurfaces from each other, colors were assigned arbitrarily to the isosurfaces after the extraction procedure. A section of the isosurface was then selected in the proximal medulla (highlighted in red and indicated by a white arrow) for examination of column coverage using Csp2a as a reference for medulla columns (A2). An array of eight columns (white square) surrounding a central column was used as a reference frame to estimate contiguity of the columns covered by the selected isosurface area (dashed line).

(D) Projection of all the registered isosurfaces for each RhTmY cell type on the reference optic lobe (n = 4 for Rh3TmY and Rh6TmY, n = 5 for Rh4TmY and Rh5TmY).

(E) The number of isosurfaces analyzed in (D) as well as the number of neurons labeled per isosurface are shown in the table.

(F) Quantification of column coverage. Percentage of contiguity was calculated as (c-h) *100/c where c is the number of columns covered by the area of the TmY isosurface and h is the number of columns not covered by the TmY isosurface area (see Supplemental Experimental Procedures). Error bars denote ± SEM. See also Figures S6 and S7.

of multiple Rh3 TmY neurons in 108 flies reveals a highly stereotyped pattern of projections to the lobula complex. Rh3 TmY neurons branch to extend axons to both the lobula plate and lobula. In the lobula plate, the processes innervate all four layers in a columnar fashion, presumably maintaining retinotopy (Figures 7 and S6). Occasionally the main branch splits into two with each branch exhibiting arborizations in different layers of the lobula plate. A similar pattern of projections to the lobula plate is observed for the four different TmY cells. In contrast to the projections in the lobula plate, the projections of all the TmY variants extend to the innermost layer in the lobula and have strikingly similar patterns that are conserved across animals. The axonal projections in the lobula appear far simpler than the rich arborizations in the lobula plate (Figures 6B and 6C) and the projection patterns appear similar for each of the four distinct TmY cell types. This is distinct from the unique patterns of projection exhibited by the four TmYs in the proximal medulla (Figure 6A and see below).

We further analyzed the TmY projections by Sholl analysis to provide a more quantitative assessment of the branching topology. Sholl intersections of branching topology of the traced neurites were then subjected to hierarchical cluster analysis. Semi-automated neuron tracing reveals that each of the TmY cells exhibits distinct processes in medullary layers 7–10. In contrast, each of the TmY variants projects to the innermost layer of the lobula and the four layers of the lobula plate. The four TmYs exhibit strikingly similar projection patterns that are conserved across animals (Figures 6B and 6C). The proximal medullary projections of the TmY cells cluster into four groups that correspond to their four presynaptic partners (Figure 6D). The lobula and lobula plate projections define two distinct clusters with each of these clusters comprising all four TmY cell type processes (Figure 6E). These findings are in accord with the observation that the four distinct TmY cells each reveal distinct medullary processes and synapse with the different chromatic photoreceptor neurons but project to similar loci in the lobula and lobula plate.

## Topographic Organization of TmY Cells in the Medulla and Lobula Complex

We examined the spatial organization of the TmY cell projections in the proximal medulla and the downstream lobula complex by measuring the 3D distances between multiple pairs of TmY cells in the medulla and lobula complex (Figures 7B–7D). Csp2a antibody labels distinct columns in the medulla and the lobula, allowing the analysis of topographic projections of the TmY cells in the medulla and the lobula. We find that the TmY cells contact two to three columns in the medulla (Figures 3, S3, and S4) and three columns in the lobula (Figures 6B1, 6B2, and 7A). We also observe a striking correlation of the distances between the projections of two independently labeled TmY cells in the medulla and lobula ($R^2$ = 0.9, Figure 7E). These data suggest that four overlapping topographic maps of color signals exist in the medulla, and are maintained in the projections to the lobula complex.

## TmY Cells Respond to Selective Activation of Their Presynaptic Partners

Tango-Trace has permitted the identification of four postsynaptic partners of the four chromatic photoreceptor neurons. We have developed calcium-imaging procedures to verify that the individual TmY cells are synaptically connected to the different photoreceptor subtypes. The heat-sensitive channel, dTrpA1, was expressed in the individual photoreceptors and calcium responses were recorded in the postsynaptic partners labeled by Tango-Trace in response to heat activation. A modified imaging procedure (Clark et al., 2011) was developed to expose the fly eye to local heat with a temperature controlled copper wire placed on the anterior surface of the fly head. The cuticle was then removed on the posterior surface of the fly head, rendering the optic lobe accessible to two-photon microscopy (Figure 8A). Stimulation consisted of a short 3 s heat pulse applied during a 60 s imaging period. Prestimulation images acquired 3 s before the heat pulse were used to calculate the baseline fluorescence of labeled cells. We imaged responses of photoreceptor axon termini in the medulla and the responses of axon termini of TmY cells in the lobula plate.

In initial experiments, we expressed the genetically encoded calcium indicator TN-XXL (Mank et al., 2008) in cells postsynaptic to yR7 cells using HA-Tango-Trace. TN-XXL was also expressed in yR7 photoreceptors under the control of *Rh4* Gal4. We present average responses of Rh4TmY cells in the lobula plate and yR7 cells in the medulla. Heat activation of yR7 cells selectively expressing dTrpA1 elicited increases in $Ca^{2+}$ in yR7 cells and decreases in $Ca^{2+}$ cells in the lobula plate projections of Rh4TmY cells (Figures 8D1 [n = 34], 8D5 [n = 32], and 8E [$p < 0.0001$]). The increase in fluorescence in photoreceptors is consistent with dTrpA1-mediated depolarization, whereas the decrease in fluorescence in Rh4TmY is in accord with hyperpolarization resulting from activation of ort, the HA responsive $Cl^-$ channel.

In these experiments, the calcium indicator was expressed using HA-Tango-Trace, precluding internal controls for the specificity of connections. We therefore performed a second set of imaging experiments in which we expressed TN-XXL in a Gal4 line, *GMR27A06-Gal4* that labels Rh4TmY cells (Jenett et al., 2012). This Gal4 line also labels T1 cells in the lamina and the medulla (Figure S8E), but the projections of T1 cells were spatially separated from the Rh4TmY cells, allowing us to distinguish the two cell types. In these flies, heat activation of yR7 cells selectively expressing dTrpA1 elicited decreases in $Ca^{2+}$ in the imaged regions of Rh4TmY cells similar to the HA-Tango-Trace labeled Rh4TmY cells (Figures 8D3 [n = 31], and 7E [$p > 0.1$]). The $Ca^{2+}$ response in Rh4TmY cells was specific for yR7 activation and was not observed with activation of yR8 cells that send inputs to the same columns in the medulla (Figures 8D3 [n = 31], 8D4 [n = 22], and 8E [$p < 0.0001$]). $Ca^{2+}$ responses were not observed in either yR7 or Rh4TmY cells in control flies that did not express dTrpA1 in yR7 cells. The responses of the postsynaptic partners of yR7 cells in the lobula plate were sustained in contrast to the transient responses of yR7 cells in the medulla. Furthermore, these optical imaging experiments demonstrate that the TmY cells labeled by HA-Tango-Trace respond to selective activation of their presynaptic partners. Therefore, HA-Tango-Trace labels specific functional connections in the visual system.

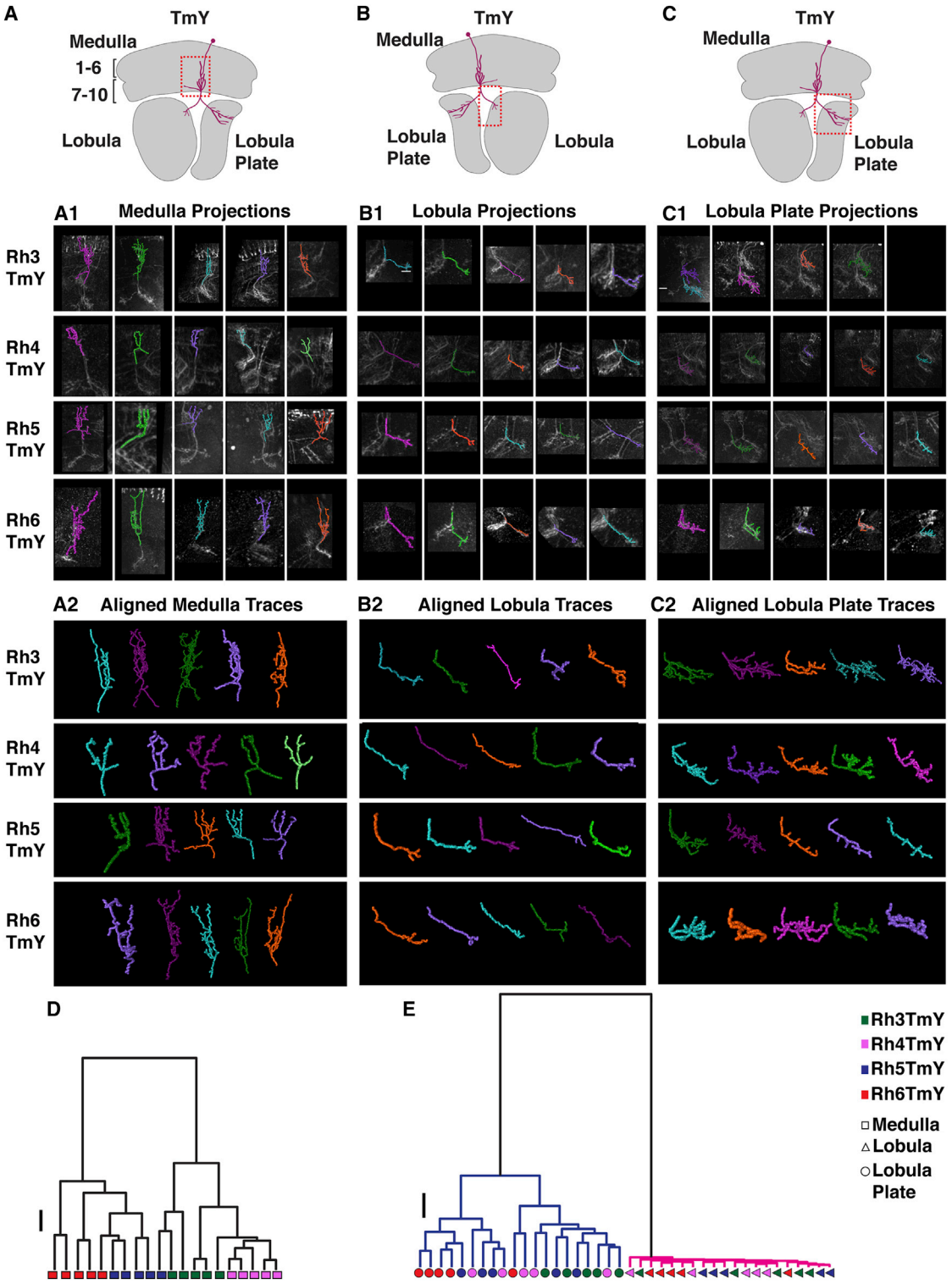


**Figure 6. Semi-Automated Neurite Tracings of TmY Cells in the Proximal Medulla and the Lobula Complex**

(A) Projections from TmY cells postsynaptic to the different photoreceptor subtypes are distinct in the proximal medulla. The projections from sparsely labeled TmY cells can be seen as they course through the proximal medulla, branch, and extend processes to the lobula and lobula plate. TmYs that connect to p/y R7 and R8 exhibit distinct arborizations in the proximal medulla. Individual TmY projections in the proximal medulla that connect to the inner photoreceptors in the medulla were followed into the lobula complex in different flies (A1–A8).

*(legend continued on next page)*

## DISCUSSION

We developed a genetic strategy, Tango-Trace, that permits the identification of postsynaptic neurons within a circuit in the fly brain. The use of Tango-Trace in the fly optic lobe has allowed us to identify postsynaptic partners of each of the four different chromatic photoreceptors. The stochastically distributed inner photoreceptor subtypes each contact a unique postsynaptic TmY cell. The TmY cells, although anatomically distinct in the proximal medulla, share several anatomic features in the lobula and lobula plate. In the lobula plate, each TmY projects to all four layers, whereas in the lobula, arborizations are restricted to the innermost layer. Moreover, each of the four different TmY cells maintains a retinotopic map from the medulla to the lobula complex. Registered images of isosurfaces of different TmYs show that contiguous maps are likely to overlap. Thus, four overlapping topographic maps transmit different color information from individual inner photoreceptor subtypes in the retina to the lobula complex. These observations demonstrate that the four inner photoreceptor subtypes process chromatic visual information in separate and parallel pathways. A given photoreceptor, however, cannot distinguish wavelength differences from intensity differences and color vision therefore requires that signals from the different dedicated TmYs are compared by convergent processing downstream.

In the trichromatic mammalian retina, each of the different cones synapse on a different bipolar cell, a feature most clearly illustrated by the S-type cones that synapse on postsynaptic S-ON bipolar cells (Masland, 2001). Thus, independent parallel information channels continue from the cone to bipolar cell and L versus M opponency, as well as L-M versus S opponency is observed in the retinal ganglion cells (Nassi and Callaway, 2009). This functional organization in the mammalian retina resembles the parallel channels between the inner photoreceptors of the fly and the four TmY cells. Opponency in *Drosophila* would therefore be apparent in downstream targets including the proximal medulla or lobula complex. In the honeybee, several types of color opponent neurons have been detected by electrophysiologic recordings in the medulla and lobula (Kien and Menzel, 1977; Yang et al., 2004), two sites of axon arborization we observe for the four TmY cells. Whatever the site of integration of the four distinct photoreceptor channels, the identification of independent output neurons for the four photoreceptor types suggests an anatomic substrate for the integration necessary for color analysis.

Individual inner photoreceptors express only one of the four rhodopsin subtypes, dictated by the stochastic expression of specific transcription factors (Chou et al., 1996, 1999; Franceschini et al., 1981; Mikeladze-Dvali et al., 2005; Papatsenko et al., 1997; Wernet et al., 2006). Each photoreceptor then projects retinotopically to a single column in the medulla (reviewed in Melnattur and Lee, 2011). The stochastically distributed photoreceptor subtypes then contact a unique postsynaptic TmY target with precision. How is this map established? In one model, all columns might contain dendrites from all four potential TmY targets, but an identity code of synaptic specificity cues between photoreceptors and TmY cells assures that only the correct synapses form. Alternatively, each photoreceptor subtype may induce the differentiation of its cognate TmY target, thereby matching pre- and postsynaptic partners. Finally, the specificity of connections may be initiated by columnar guidance cues and TmY receptors.

The four TmY cells postsynaptic to each of the chromatic photoreceptor types arborize across all layers of the lobula plate and this may afford a new site of integration of inner and outer photoreceptor signals. Inner photoreceptors provide inputs to motion-sensitive pathways by forming direct, electrical connections with the axon terminals of outer photoreceptors, enhancing the robustness of motion vision (Wardill et al., 2012). These connections arise at an early stage in visual processing that necessarily precedes comparisons between inner photoreceptor signals and therefore cannot provide color information to motion detecting circuits. Rather, these early connections can broaden the spectral tuning of these pathways. The lobula plate outputs of the TmY cells we have identified may act redundantly with these peripheral interactions, providing another neural mechanism to enhance motion detection. However, as the arbors of these TmY cells span small numbers of neighboring columns in the proximal medulla, these cells might also represent a site of integration between different spectral inputs. Thus, the projections of these cells to the lobula plate could relay spatially restricted information about color to motion sensitive areas.

(B and C) Individual TmY cell projections in the lobula (B1–B7) and lobula plate (C1–C8) were followed from the proximal medulla in different flies. A striking similarity in projection pattern is observed among the four different TmYs. TmY neurons branch to extend processes to both the lobula plate and lobula. (B) In the lobula plate, the processes innervate all four layers. Occasionally the main branch splits into two with each branch exhibiting arborizations in different layers of the lobula plate. (C) In the lobula, projections of the all the TmY variants extend to the innermost layer in the lobula and have a strikingly similar projection pattern that was conserved across animals. The generation of sparse-labeled TmYs and the staining was performed as described in Figure 3. Semi-automated neurite tracings of TmY cells were performed using the skeleton tree algorithm in Amira (see Supplemental Experimental Procedures). To distinguish the traced neurites from each other, colors were assigned arbitrarily to the skeleton after the tracing procedure. The process entering the lobula complex was chosen as the reference point for alignment in Amira. Tracings were both aligned along principal axes in 3D using rigid transformation as well as manually aligned along the axes of the process entering the lobula complex. Scale bars represent 10 μm.

(D) A vertical hierarchical dendrogram groups the TmYs in four different clusters according to their similarity in projection patterns in the proximal medulla. The Sholl intersections of the aligned traces from (A) were selected for subsequent cluster analysis (see Supplemental Experimental Procedures). These four clusters coincide with the four corresponding presynaptic photoreceptor subtypes. The linkage calculation is based on Euclidian distance using Ward's method. Vertical bars represent 20 units in Euclidean distance.

(E) A hierarchical cluster analysis as described in (D) was performed on the Sholl intersections of the aligned traces from (B) and (C). The cluster analysis groups TmYs in two different clusters according to their projection patterns in the lobula complex. The two clusters correspond to the processes of the TmY cells projecting to the most medial layer of the lobula and all the four layers of the lobula plate with no apparent cell type specific clustering. Vertical bars represent 20 units in Euclidean distance.

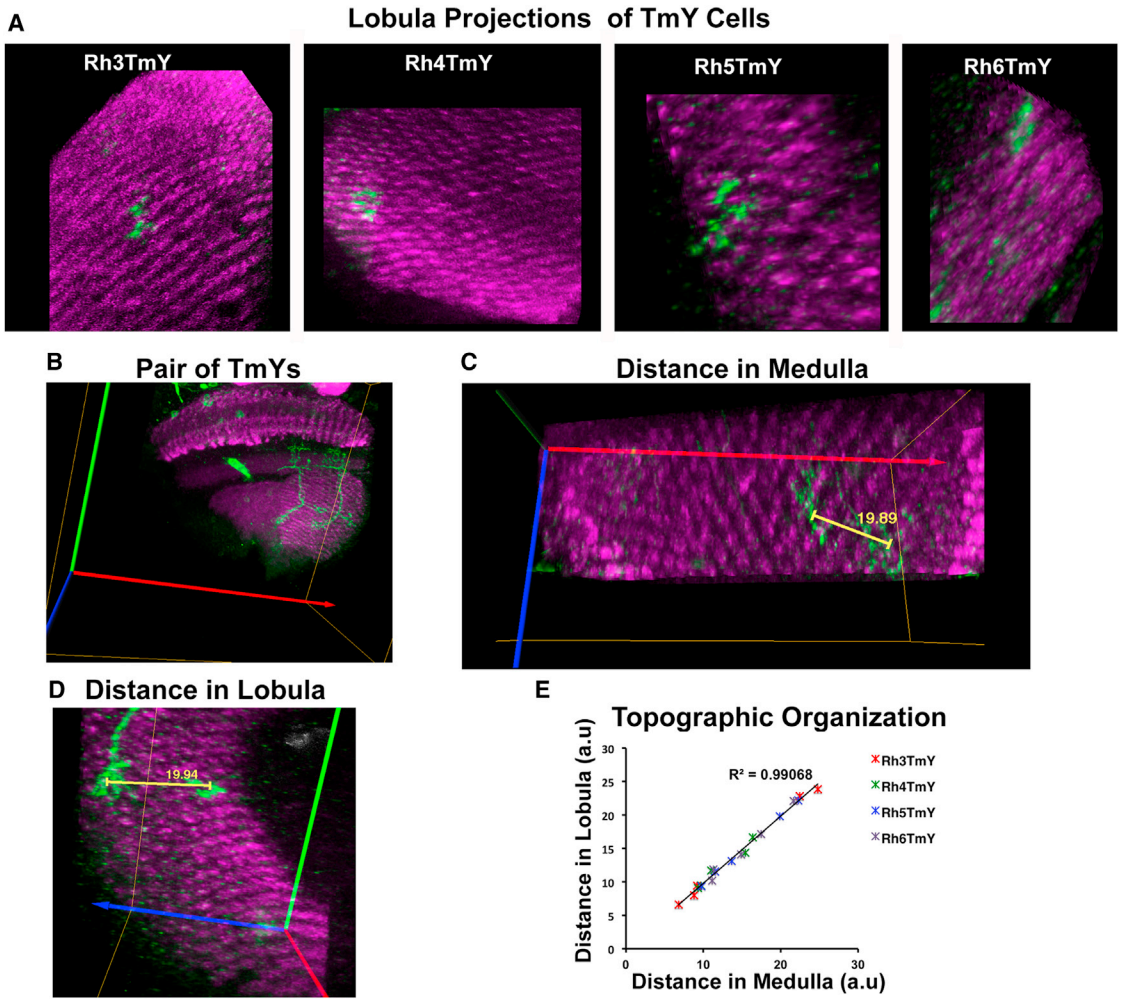


**Figure 7. Topographic Organization of TmY cells in the Medulla and Lobula Complex**

(A) Projections of TmY cells in the lobula. Brains were immunostained with anti-GFP (green), and the neuropil marker anti-Csp2a (magenta). Images were rendered in Amira for measurement of distances between projections of two cells in the proximal medulla and lobula.

(B) A representative image of a pair of Rh5TmY labeled by HA-Tango-Trace.

(C and D) Representative images to illustrate the distance measurements between projections in proximal medulla and lobula performed using the 3D measurement tool in Amira (see Supplemental Experimental Procedures) for all the RhTmY cell types (n = 5 for each cell type). Three principal axes of the image volume are denoted by red, blue, and green.

(E) A correlation plot of the distances of all the RhTmY pairs. x axis denotes the 3D distance in amira units (a.u) in medulla and y axis denotes the 3D distance in a.u. in the lobula.

See also Figures S6 and S7.

Although turning responses evoked by optic flow are color insensitive (Yamaguchi et al., 2008), lobula plate neurons in fruit flies and larger Diptera can be tuned to motion in different directions, complex patterns of optic flow, as well as looming objects (de Vries and Clandinin, 2012; Hausen, 1982; Joesch et al., 2008; Krapp and Hengstenberg, 1997). Moreover, distinct motion sensitive circuits guide different behavioral responses (Duistermars et al., 2012; Duistermars and Frye, 2008; Katsov and Clandinin, 2008; Silies et al., 2013). Thus, the pathways defined by these TmY cells might adjust the sensitivity of lobula plate neurons to motion in a color-dependent fashion, providing a mechanism for tuning particular motion-sensitive behaviors to specific spectral environments.

Tango-Trace was developed to identify postsynaptic targets of the chromatic photoreceptor neurons. The modular design of Tango-Trace allows a more general application to identify postsynaptic partners of virtually any genetically defined subpopulation of presynaptic cells. A variant Tango mapping approach has been developed to identify sites of dopamine-mediated neuromodulation in the brain (Inagaki et al., 2012). The only requirement for Tango tracing is the knowledge of the neurotransmitter released by the presynaptic neuron allowing the identification and genetic modification of its cognate GPCR essential for Tango-Trace. Tango-Trace affords several advantages as a general approach to trace neural pathways in the fly brain. First, the identification of postsynaptic targets

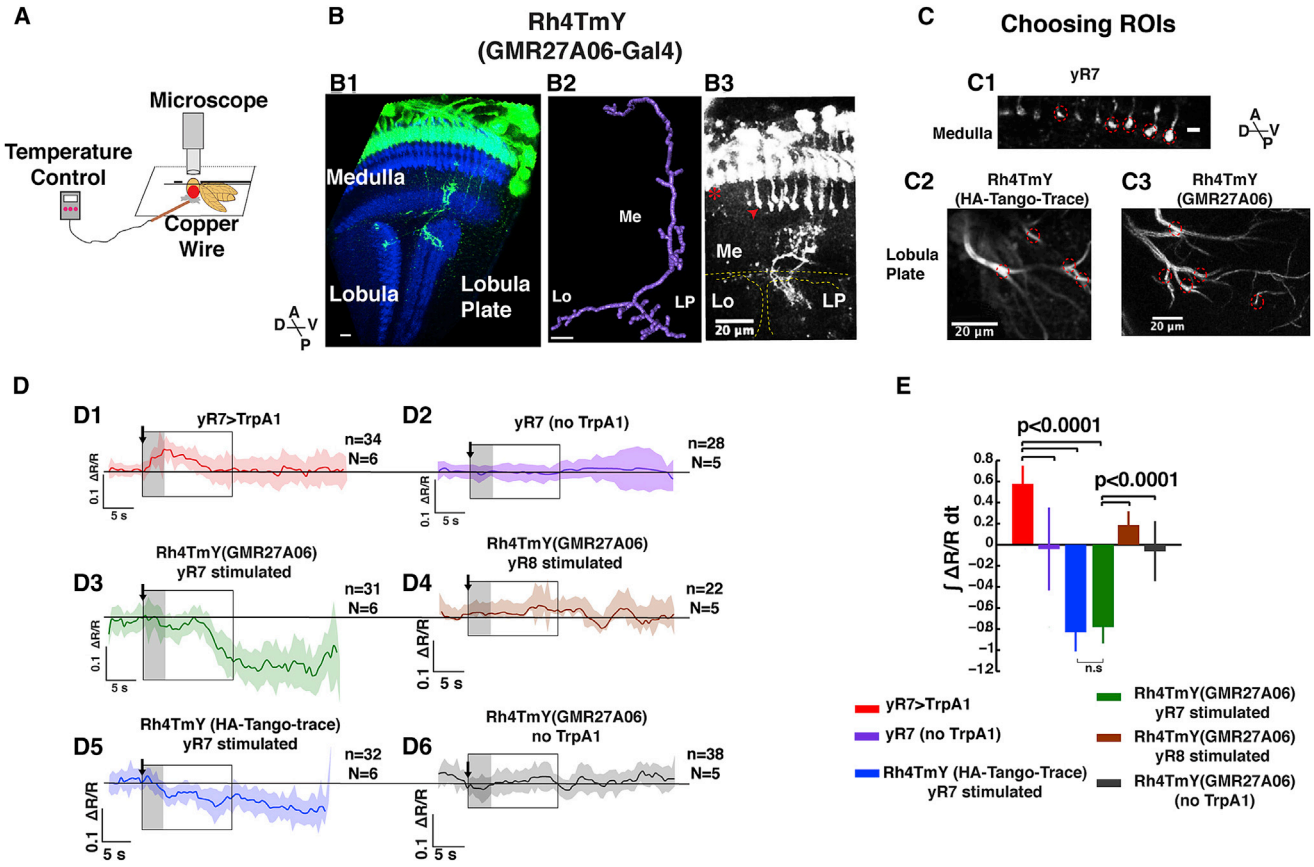


**Figure 8. Imaging the Responses of TmY Cells to Activation of Their Presynaptic Partners**

(A) Schematic illustration of the two-photon calcium imaging strategy used to record responses in Rh4TmY while activating yR7 and yR8 expressing dTrpA1 (see Experimental Procedures).

(B) *GMR27A06-Gal4* labels Rh4TmY cells in the optic lobe. (B1) Confocal image of *GMR27A06-Gal4* expressing CD8-GFP. (B2) Semi-automated neurite tracing of Rh4TmY from (B1). (B3) A two-photon image of the optic lobe of a fly expressing TN-XXL driven by *GMR27A06-Gal4* and *Rh4 Gal4*. In these brains, TN-XXL is expressed in Rh4TmY as well as yR7 (arrowhead) and T1 (asterisk). The brains in B1 were immunostained to depict CD8GFP labeling with anti-GFP (green), neuropil marker anti-Csp2a (blue), and photoreceptor marker mAb24B10 (red). Scale bar represents 10 μm; 20 μm in (B3).

(C) Regions of interest (ROIs) exhibiting bright fluorescence in the yR7 axon termini in the medulla and Rh4TmY axon termini in the lobula plate were identified using the live data mode of the two-photon microscope. Baseline fluorescence of TN-XXL illustrating the ROIs chosen for imaging in the medulla for photoreceptor axon termini in the M6 layer (C1) and in the lobula plate for Rh4TmY axon termini labeled by HA-Tango-Trace in (C2) and *GMR27A06-Gal4* in (C3). Scale bar in (C1) represents 5 μm and 20 μm in (C2) and (C3).

(D1–D6) Average traces depicting changes in fluorescence due to calcium responses in ROIs identified in (C) elicited by heat activation of yR7 and yR8 expressing dTrpA1.

(D1) yR7 cells expressing dTrpA1 driven by *Rh4 Gal4* exhibit significant increases in fluorescence elicited by heat activation without responding even weakly when they do not harbor the dTrpA1 transgene (D2).

(D3) Rh4TmY cells expressing TN-XXL driven by *GMR27A06-Gal4* selectively exhibit decreases in $Ca^{2+}$ in the imaged regions elicited by heat-activation of yR7 cells expressing dTrpA1. The $Ca^{2+}$ response in Rh4TmY was not observed with activation of yR8 cells (D4) or heat activation of yR7 that do not harbor the dTrpA1 transgene (D6).

(D5) Rh4TmY cells expressing TN-XXL driven by HA-Tango-Trace exhibit decreases in $Ca^{2+}$ with heat activation of yR7. Shading denotes ± SEM, n denotes the number of ROIs imaged, and N denotes the total number of flies imaged per genotype. The arrow indicates the onset of the heat pulse. The gray shaded box denotes the period of the 3 s heat pulse and the black open box denotes the period chosen for quantification in (E).

(E) Quantification of fluorescence changes. Integrated responses ( $\int \Delta R/R.dt$ ) for 15 s after the onset of the heat pulse as denoted by the black open box in each trace in (D). p Values represent Wilcoxon rank-sum test. Error bars denote ± SEM.

See also Figure S8.

relies on exogenous genes introduced into the fly to create a novel signaling pathway independent of the activation of potential confounding endogenous cell-signaling events. Moreover, this approach transforms rapidly adapting signaling events into a more stable and amplifiable cellular response. In addition, the transcriptional readout of the Tango system not only permits the expression of reporters that allow the visualization of neurons, but also manipulatable effectors including ion channels as well as $Ca^{2+}$ indicators in restricted populations of postsynaptic neurons. Tango-Trace has particular

advantages in the fly brain where tangled neuropils, without apparent structure, predominate and the anatomic proximity of processes cannot reliably predict functional connections. GRASP (Feinberg et al., 2008), which depends upon synaptic level proximity, affords an alternative tracing approach but does not directly report a functional synapse, an important feature inherent in Tango-Trace.

One concern remaining with the Tango approach surrounds the question of sensitivity. We detected four TmY cells and two interneurons, Dm8 and Mia, postsynaptic to the inner photoreceptors. We do not know the complete repertoire of neurons in the medulla, postsynaptic to the inner photoreceptors and therefore cannot determine the effectiveness of labeling for all postsynaptic targets. Over 70 neuronal cell types have been identified in the medulla and the identification of direct targets of R7 and R8 by electron microscopic reconstruction has preliminarily described Dm8, Tm5, Tm9 (Gao et al., 2008) as well as L1, L2, L3, Dm2, Mi4, Mi9, Mi15, and Tm20 as postsynaptic targets (Takemura et al., 2013). At present, the EM reconstruction of medulla columns is incomplete because current efforts have focused on the circuits involved in motion detection downstream of outer photoreceptors (Takemura et al., 2013). Thus, resolution of apparent discrepancies among the various EM reconstruction efforts, and between the EM data and Tango trace, may emerge upon a complete EM reconstruction of a medulla column. The inability to detect targets other than the four TmYs in Tango-Trace may reflect inefficiencies or bias in the identification of postsynaptic targets. This notwithstanding, the identification of the four distinct TmYs and the independent confirmation of their connectivity by functional imaging argues strongly for their participation in specific parallel pathways postsynaptic to the chromatic photoreceptors.

## EXPERIMENTAL PROCEDURES

### Fly Stocks

*UAS dTrpA1* lines were generously provided by Paul Garrity (Hamada et al., 2008); *hs-Flp; tubp > Gal80,y+ >* transgenic flies were provided by Gary Struhl (Columbia University). We also used *Rh3 Gal4* on II, *Rh4 Gal4* on II, *Rh5 Gal4* on II and *Rh6 Gal4* on III, *P(neoFRT)19A, P(tubP-GAL80)LL1, P(hsFLP)1, w[*]; P(UAS-mCD8::GFP)LL5;* (Bloomington Stock Center), *y[1]w[1118] P(neoFRT)19A;;* (Bloomington Stock Center), *w[*]; noc[Sco]/CyO; P(tubP-GAL80$^{ts}$)7* (Bloomington Stock Center), and *GMR27A06-Gal4* on III (Bloomington Stock Center).

### Fly Husbandry

*Drosophila* stocks were reared on standard cornmeal-agar-dextrose medium at 25°C. *W1118* or *yw* strains were used for transgene injections. P-element mediated germline transformations and genetic manipulations were performed using standard techniques. Transgene injections were performed by BestGene.

### HA-Tango-Trace labeling

Flies were reared in ambient light conditions to keep any light-induced activity at low-levels in all HA-Tango-Trace labeling experiments and then exposed to heat for dTrpA1 activation (see below). Flies were then shifted to 25°C overnight, fixed, and stained. Sparse MARCM clones were generated by a 30 min heat shock every day from early larval to late pupal stages during development to maximize the number of labeled cell types. Activation of photoreceptors expressing dTrpA1 was then achieved by a heat-cool cycle by gradually warming these flies from 25°C to 37°C for 15 min followed by 5 min cooling. This cycle was repeated for 2 hr.

### Tubulin-Gal80$^{ts}$ inactivation

Flies carrying the HA-Tango transgenes and the Tubulin-Gal80$^{ts}$ transgene were first shifted to 30°C for at least 18 hr to inactivate the Gal80 protein and then stimulated with light, incubated overnight at 25°C and immunostained.

### Immunocytochemistry and Confocal Microscopy

Fly heads were fixed in 2% formaldehyde in phosphate-buffered lysine (PBL) for 2 hr at room temperature, and washed three times for 15 min in PBS + 0.3% TX-100. Microdissection was performed in PBST to remove the cuticle and connective tissues. Samples were blocked for 30 min in 10% normal goat serum. Primary and secondary incubations were performed overnight at 4°C, with shaking. Samples were incubated for 30 min in 10% normal goat serum, then in a cocktail of primary antibodies including a mouse anti-nc82 (1:20, DSHB), mouse anti-DCsp-2a (1:20, DSHB), mouse mAb24B10 (1:10, DSHB), Abcam chicken anti-GFP (1:1,000) overnight. Samples were washed three times for 10 min with PBST before incubation for 3 hr with a cocktail of secondary antibodies, which include goat anti-mouse conjugated with Alexa Fluor 568 (1:1,000), goat anti-chicken conjugated with Alexa Fluor 488 (1:1,000), and a 1:1,000 dilution of TOTO-3 (Molecular Probes). After three 10 min rinses with PBST, brains were mounted in Vectashield (Vector Labs) and imaged. Image stacks were taken either with Zeiss 510 Meta laser scanning confocal microscope or Leica TCS SP2 AOBS confocal microscope using a 40× (NA = 1.25) lens.

### Calcium Imaging and Image Analysis

Flies expressing *UAS-TN-XXL* were immobilized and mounted as previously described (Clark et al., 2011). A custom designed heating device (Warner Instruments) with a copper wire connected to a temperature control was used to provide local heat to the retina. The copper wire was glued to the retina on the anterior side of the fly with an epoxy thermal glue (Arctic Silver Alumina two part thermal adhesive compound epoxy) to avoid air gaps and facilitate efficient heat transfer to the eye. The epoxy glue was allowed to set for 30 min before the imaging session was started. A 3 s 30°C heat pulse was provided to the eye at the 25th second during a 60 s imaging period while the brain was exposed to a flowing saline bath. Prestimulation images acquired 3 s before the heat pulse were used to calculate the baseline fluorescence of labeled cells. Two-photon imaging was carried out with a Leica TSC SP5 II two-photon microscope, using a Leica HCX APO 20×/1.0 NA water immersion objective (Leica) and a Chameleon femtosecond laser (Coherent). The excitation wavelength was set to 830 nm and ~10–20 mW of power was applied at the sample. CFP- and citrine-emitted photons were collected using two emission filters and a 495-LP beam splitter (Semrock). Regions of interest (ROIs) exhibiting bright fluorescence were identified using the LAS AF Live Data Mode from Leica. Acquisition of time series of images was done at a constant rate (frame size of 200 × 50 pixels and a line rate of 150 Hz in unidirectional scanning mode) to allow collection of images at ~2 Hz for durations of 60 s. Preliminary experiments demonstrated that the longest responses elicited by the heat pulse dissipated by 1.5 min. The presentation of consecutive heat pulses in the same fly was therefore separated by at least 2 min. A typical imaging experiment lasted 30 min per animal. Average traces of responses (ΔR/R) 5 s before the stimulus onset till the end of the 60 s imaging period (40 s in total) were used for analysis.

Image analysis was done in a custom written Matlab code as previously described (Clark et al., 2011) by manually choosing ROIs. Average traces were generated from raw t-series signal ratios for all genotypes. The traces were smoothed using a 7-point moving average method in Matlab (Figure S8) to demonstrate the average responses for all data. Integrated responses $\left(\int \Delta R/R.dt\right)$ for 15 s after the onset of the heat pulse were calculated by computing the area under the curve for all the average traces of all genotypes using the trapz function incorporated in Matlab. Integrated responses were calculated for all the ROIs for every fly, and the fly means were used to calculate the average integrated responses and SEM.

## SUPPLEMENTAL INFORMATION

Supplemental Information includes Supplemental Experimental Procedures and eight figures and can be found with this article online at http://dx.doi.org/10.1016/j.neuron.2014.06.025.

## ACKNOWLEDGMENTS

We thank Paul Garrity, Gary Struhl, Wes Grueber, and members of the Axel lab and Clandinin lab for reagents and helpful discussions; members of the Clandinin lab for assistance with 2-photon microscopy; and Phyllis Kisloff, Miriam Gutierrez, and Adriana Nemes for assistance with general laboratory concerns and the preparation of this manuscript. Financial support was provided by the Gates Foundation: Grand Challenges in Global Health (FNIH-798; to R.A. and S.J.), R01 EY022638 (to T.R.C.), R01 MH086920 (to G.B.), and the Howard Hughes Medical Institute (to R.A.).

Accepted: June 18, 2014
Published: July 17, 2014

## REFERENCES

Barnea, G., Strapps, W., Herrada, G., Berman, Y., Ong, J., Kloss, B., Axel, R., and Lee, K.J. (2008). The genetic design of signaling cascades to record receptor activation. Proc. Natl. Acad. Sci. USA *105*, 64–69.

Buchner, E., Buchner, S., and Bülthoff, H. (1984). Identification of [3H]deoxyglucose-labelled interneurons in the fly from serial autoradiographs. Brain Res. *305*, 384–388.

Buchner, E., Buchner, S., Burg, M.G., Hofbauer, A., Pak, W.L., and Pollack, I. (1993). Histamine is a major mechanosensory neurotransmitter candidate in Drosophila melanogaster. Cell Tissue Res. *273*, 119–125.

Chou, W.H., Hall, K.J., Wilson, D.B., Wideman, C.L., Townson, S.M., Chadwell, L.V., and Britt, S.G. (1996). Identification of a novel Drosophila opsin reveals specific patterning of the R7 and R8 photoreceptor cells. Neuron *17*, 1101–1115.

Chou, W.H., Huber, A., Bentrop, J., Schulz, S., Schwab, K., Chadwell, L.V., Paulsen, R., and Britt, S.G. (1999). Patterning of the R7 and R8 photoreceptor cells of Drosophila: evidence for induced and default cell-fate specification. Development *126*, 607–616.

Clandinin, T.R., and Zipursky, S.L. (2002). Making connections in the fly visual system. Neuron *35*, 827–841.

Clark, D.A., Bursztyn, L., Horowitz, M.A., Schnitzer, M.J., and Clandinin, T.R. (2011). Defining the computational structure of the motion detector in Drosophila. Neuron *70*, 1165–1177.

de Vries, S.E.J., and Clandinin, T.R. (2012). Loom-sensitive neurons link computation to action in the Drosophila visual system. Curr. Biol. *22*, 353–362.

Duistermars, B.J., and Frye, M. (2008). A magnetic tether system to investigate visual and olfactory mediated flight control in Drosophila. J. Vis. Exp. (21)

Duistermars, B.J., Care, R.A., and Frye, M.A. (2012). Binocular interactions underlying the classic optomotor responses of flying flies. Front. Behav. Neurosci. *6*, 6.

Farrow, K., Haag, J., and Borst, A. (2003). Input organization of multifunctional motion-sensitive neurons in the blowfly. J. Neurosci. *23*, 9805–9811.

Feinberg, E.H., Vanhoven, M.K., Bendesky, A., Wang, G., Fetter, R.D., Shen, K., and Bargmann, C.I. (2008). GFP Reconstitution Across Synaptic Partners (GRASP) defines cell contacts and synapses in living nervous systems. Neuron *57*, 353–363.

Fischbach, K.F., and Dittrich, A.P.M. (1989). The optic lobe of *Drosophila melanogaster*. I. A Golgi analysis of wild-type structure. Cell Tissue Res. *258*, 441–475.

Franceschini, N., Kirschfeld, K., and Minke, B. (1981). Fluorescence of photoreceptor cells observed in vivo. Science *213*, 1264–1267.

Gao, S., Takemura, S.-Y., Ting, C.-Y., Huang, S., Lu, Z., Luan, H., Rister, J., Thum, A.S., Yang, M., Hong, S.-T., et al. (2008). The neural substrate of spectral preference in Drosophila. Neuron *60*, 328–342.

Gengs, C., Leung, H.T., Skingsley, D.R., Iovchev, M.I., Yin, Z., Semenov, E.P., Burg, M.G., Hardie, R.C., and Pak, W.L. (2002). The target of Drosophila photoreceptor synaptic transmission is a histamine-gated chloride channel encoded by ort (hclA). J. Biol. Chem. *277*, 42113–42120.

Gisselmann, G., Pusch, H., Hovemann, B.T., and Hatt, H. (2002). Two cDNAs coding for histamine-gated ion channels in D. melanogaster. Nat. Neurosci. *5*, 11–12.

Haag, J., and Borst, A. (2003). Orientation tuning of motion-sensitive neurons shaped by vertical-horizontal network interactions. J. Comp. Physiol. A Neuroethol. Sens. Neural Behav. Physiol. *189*, 363–370.

Haag, J., and Borst, A. (2008). Electrical coupling of lobula plate tangential cells to a heterolateral motion-sensitive neuron in the fly. J. Neurosci. *28*, 14435–14442.

Hamada, F.N., Rosenzweig, M., Kang, K., Pulver, S.R., Ghezzi, A., Jegla, T.J., and Garrity, P.A. (2008). An internal thermal sensor controlling temperature preference in Drosophila. Nature *454*, 217–220.

Hausen, K. (1982). Motion sensitive interneurons in the optomotor system of the fly. II. The horizontal cells: Receptive field organization and response characteristics. Biol. Cybern. *46*, 67–79.

Heisenberg, M., and Buchner, E. (1977). The role of retinula cell types in visual behavior of *Drosophila Melanogaster*. J. Comp. Physiol. A Neuroethol. Sens. Neural Behav. Physiol. *187*, 127–162.

Hurvich, L.M., and Jameson, D. (1957). An opponent-process theory of color vision. Psychol. Rev. *64*, 384–404.

Inagaki, H.K., Ben-Tabou de-Leon, S., Wong, A.M., Jagadish, S., Ishimoto, H., Barnea, G., Kitamoto, T., Axel, R., and Anderson, D.J. (2012). Visualizing neuromodulation in vivo: TANGO-mapping of dopamine signaling reveals appetite control of sugar sensing. Cell *148*, 583–595.

Jenett, A., Rubin, G.M., Ngo, T.T., Shepherd, D., Murphy, C., Dionne, H., Pfeiffer, B.D., Cavallaro, A., Hall, D., Jeter, J., et al. (2012). A GAL4-driver line resource for Drosophila neurobiology. Cell Reports *2*, 991–1001.

Joesch, M., Plett, J., Borst, A., and Reiff, D.F. (2008). Response properties of motion-sensitive visual interneurons in the lobula plate of Drosophila melanogaster. Curr. Biol. *18*, 368–374.

Johansso, G. (1973). Visual-perception of biological motion and a model for its analysis. Percept. Psychophys. *14*, 201–211.

Katsov, A.Y., and Clandinin, T.R. (2008). Motion processing streams in Drosophila are behaviorally specialized. Neuron *59*, 322–335.

Kien, J., and Menzel, R. (1977). Chromatic properties of interneurons in optic lobes of bee 0.2. narrow-band and color opponent neurons. J. Comp. Physiol. *113*, 35–53.

Krapp, H.G., and Hengstenberg, R. (1997). A fast stimulus procedure to determine local receptive field properties of motion-sensitive visual interneurons. Vision Res. *37*, 225–234.

Lee, T., and Luo, L. (1999). Mosaic analysis with a repressible cell marker for studies of gene function in neuronal morphogenesis. Neuron *22*, 451–461.

Livingstone, M.S., and Hubel, D.H. (1984). Anatomy and physiology of a color system in the primate visual cortex. J. Neurosci. *4*, 309–356.

Mank, M., Santos, A.F., Direnberger, S., Mrsic-Flogel, T.D., Hofer, S.B., Stein, V., Hendel, T., Reiff, D.F., Levelt, C., Borst, A., et al. (2008). A genetically encoded calcium indicator for chronic in vivo two-photon imaging. Nat. Methods *5*, 805–811.

Masland, R.H. (2001). The fundamental plan of the retina. Nat. Neurosci. *4*, 877–886.

Meinertzhagen, I.A., and O'Neil, S.D. (1991). Synaptic organization of columnar elements in the lamina of the wild type in Drosophila melanogaster. J. Comp. Neurol. *305*, 232–263.

Melnattur, K.V., and Lee, C.H. (2011). Visual circuit assembly in Drosophila. Dev. Neurobiol. *71*, 1286–1296.

Melzig, J., Buchner, S., Wiebel, F., Wolf, R., Burg, M., Pak, W.L., and Buchner, E. (1996). Genetic depletion of histamine from the nervous system of Drosophila eliminates specific visual and mechanosensory behavior. J. Comp. Physiol. A Neuroethol. Sens. Neural Behav. Physiol. *179*, 763–773.

Mikeladze-Dvali, T., Wernet, M.F., Pistillo, D., Mazzoni, E.O., Teleman, A.A., Chen, Y.W., Cohen, S., and Desplan, C. (2005). The growth regulators warts/lats and melted interact in a bistable loop to specify opposite fates in Drosophila R8 photoreceptors. Cell *122*, 775–787.

Mota, T., Gronenberg, W., Giurfa, M., and Sandoz, J.C. (2013). Chromatic processing in the anterior optic tubercle of the honey bee brain. J. Neurosci. *33*, 4–16.

Nassi, J.J., and Callaway, E.M. (2009). Parallel processing strategies of the primate visual system. Nat. Rev. Neurosci. *10*, 360–372.

Papatsenko, D., Sheng, G., and Desplan, C. (1997). A new rhodopsin in R8 photoreceptors of Drosophila: evidence for coordinate expression with Rh3 in R7 cells. Development *124*, 1665–1673.

Paulk, A.C., and Gronenberg, W. (2008). Higher order visual input to the mushroom bodies in the bee, Bombus impatiens. Arthropod Struct. Dev. *37*, 443–458.

Paulk, A.C., Phillips-Portillo, J., Dacks, A.M., Fellous, J.M., and Gronenberg, W. (2008). The processing of color, motion, and stimulus timing are anatomically segregated in the bumblebee brain. J. Neurosci. *28*, 6319–6332.

Paulk, A.C., Dacks, A.M., Phillips-Portillo, J., Fellous, J.M., and Gronenberg, W. (2009). Visual processing in the central bee brain. J. Neurosci. *29*, 9987–9999.

Raghu, S.V., and Borst, A. (2011). Candidate glutamatergic neurons in the visual system of Drosophila. PLoS ONE *6*, e19472.

Riehle, A. (1981). Color Opponent Neurons of the Honeybee in a Heterochromatic Flicker Test. J. Comp. Physiol. *142*, 81–88.

Roeder, T. (2003). Metabotropic histamine receptors—nothing for invertebrates? Eur. J. Pharmacol. *466*, 85–90.

Rushton, W.A. (1972). Pigments and signals in colour vision. J. Physiol. *220*, 1P–31P.

Sanes, J.R., and Zipursky, S.L. (2010). Design principles of insect and vertebrate visual systems. Neuron *66*, 15–36.

Sarthy, P.V. (1991). Histamine: a neurotransmitter candidate for Drosophila photoreceptors. J. Neurochem. *57*, 1757–1768.

Shaw, S.R. (1984). Early visual processing in insects. J. Exp. Biol. *112*, 225–251.

Silies, M., Gohl, D.M., Fisher, Y.E., Freifeld, L., Clark, D.A., and Clandinin, T.R. (2013). Modular use of peripheral input channels tunes motion-detecting circuitry. Neuron *79*, 111–127.

Stark, H. (2003). [News on the old histamine. II. Ion channels in Drosophila]. Pharm. Unserer Zeit *32*, 93.

Takemura, S.Y., Bharioke, A., Lu, Z., Nern, A., Vitaladevuni, S., Rivlin, P.K., Katz, W.T., Olbris, D.J., Plaza, S.M., Winston, P., et al. (2013). A visual motion detection circuit suggested by Drosophila connectomics. Nature *500*, 175–181.

Varija Raghu, S., Reiff, D.F., and Borst, A. (2011). Neurons with cholinergic phenotype in the visual system of Drosophila. J. Comp. Neurol. *519*, 162–176.

Wardill, T.J., List, O., Li, X., Dongre, S., McCulloch, M., Ting, C.Y., O'Kane, C.J., Tang, S., Lee, C.H., Hardie, R.C., and Juusola, M. (2012). Multiple spectral inputs improve motion discrimination in the Drosophila visual system. Science *336*, 925–931.

Wernet, M.F., and Desplan, C. (2004). Building a retinal mosaic: cell-fate decision in the fly eye. Trends Cell Biol. *14*, 576–584.

Wernet, M.F., Mazzoni, E.O., Celik, A., Duncan, D.M., Duncan, I., and Desplan, C. (2006). Stochastic spineless expression creates the retinal mosaic for colour vision. Nature *440*, 174–180.

Witte, I., Kreienkamp, H.-J., Gewecke, M., and Roeder, T. (2002). Putative histamine-gated chloride channel subunits of the insect visual system and thoracic ganglion. J. Neurochem. *83*, 504–514.

Yamaguchi, S., Wolf, R., Desplan, C., and Heisenberg, M. (2008). Motion vision is independent of color in Drosophila. Proc. Natl. Acad. Sci. USA *105*, 4910–4915.

Yamaguchi, S., Desplan, C., and Heisenberg, M. (2010). Contribution of photoreceptor subtypes to spectral wavelength preference in Drosophila. Proc. Natl. Acad. Sci. USA *107*, 5634–5639.

Yang, E.-C., Lin, H.-C., and Hung, Y.-S. (2004). Patterns of chromatic information processing in the lobula of the honeybee, Apis mellifera L. J. Insect Physiol. *50*, 913–925.